obtained for the as-welded and stress-relieved specimen sets respectively. In the case of the as-welded MMA specimens (Figure 4.8 (a)), 68 of the 112 predicted defect sizes would have led to the defect being considered safe under what was, in fact, failure conditions. Similarily, in Figure 4.8 (b) (as-welded SA test plates), 104 of the 116 predicted defects would have been assessed as non-critical under the applied failure loads. This corresponds to 61% and 90% of the critical defect sizes being incorrectly assessed. Considering the same analysis for the stress-relieved specimen sets (Figure 4.9 (a) and (b)); 37 (or 63%) of the 59 predicted defect sizes in the MMA welds would have led to an erroneous assessment of safe conditions, and in the SA welds, 52 (or 88%) of the 59 defects would have been incorrectly assessed. (These results were established on the basis that the experimental assessment lines defining critical conditions).

It therefore appears that the SA welds are somewhat less tolerant to the ultrasonic defect sizing variability than the MMA welds, both in the as-welded and stress-relieved condition. It will be recalled from the previous Section that in the prediction of failure stress levels using the PD 6493 assessment, the stress-relieved MMA material was the most affected by the UT defect sizing variability. It is considered that this apparent discrepancy is most likely due to the fact that there is no stipulated recategorisation of near surface flaws in the R-6 approach.

Unlike the PD 6493 approach, there is no inherent factor of conservatism in the R-6 document. Instead, the user is encouraged to perform a sensitivity analysis (4) by varying the input data, and plotting the assessment points so obtained. The locus of these points then defines how the assessment is affected by minor changes in the various input data. This technique will also serve to indicate which of the input data effects the greatest change in the Failure Assessment Diagram, as shown in the preceding Chapter.

However, due to the large number of assessment points obtained in this work, a "global conservatism" was imposed on the Failure Assessment Diagram, to take account of innaccuracies in the UT size predictions. Thus, by replotting the assessment line between [0:0,7] and [0,7:0] in the case of the MMA specimen sets and between [0:0,5] and [0,5:0] in the case of the SA specimen sets instead of [0:1] and [1:0], all of the UT predicted defect sizes would then indicate critical conditions.

The defect size predictions as obtained in the second UT inspection programme were also used as input data in the R-6 Failure Assessment Diagram. In this second programme, it will be recalled (Chapter Two) that the operators were given more information concerning defect type and orientation, and in addition, a specific sizing procedure was stipulated. The corresponding results are shown in Figure 4.10, where it can be seen that the improved accuracy in the defect size predictions give more precise indications of defect criticalities. Of the 60 predicted defect sizes in the SA welds (Figure 4.10 (b)), only 8 (or 13%) of these indicate non-critical conditions. It will be seen from this figure, that 7 of these "non-critical" defects lie between the R-6 failure line and that postulated from the experimental failure loads and actual defect characteristics. In the case of the MMA welds (Figure 4.10 (a)) there are no such erroneous assessments.

4.3.3 Comparison of PD 6493 and R-6.

The analysis used to calculate the plastic collapse load in the R-6 assessment does not take account of ligament stability, as is required in the PD 6493 approach. It was therefore considered important to assess the compatibility of these two widely applied, yet fundamentally different, fracture mechanics defect acceptance criteria. This was achieved by considering that the UT predicted defect size which recorded the maximum failure stress for a particular test plate using the Design Curve approach of BS PD 6493 must be the least critical for that test plate, and thus it should define a point in the safe region of the R-6 Failure Assessment Diagram. In addition, the UT predicted defect that corresponded to the minimum failure stress prediction (from PD 6493) for a given testplate must be the most critical defect for that test plate, and should therefore define a point in the critical region of the Failure Assessment Diagram.

It was therefore encouraging to note that this was indeed the case, with the predicted defect which gave the minimum failure stress in the PD analyses generally defining unsafe conditions on the Failure Assessment Diagram. Similarily, the defect which gave the maximum failure stress for any given test plate invariably predicted safe conditions on the Failure Assessment Diagram. This is shown in Figure 4.11 (a) for the as-welded specimen sets, and Figure 4.11 (b) for the stress-relieved specimen sets. In both these Figures, the solid symbols indicate those defects which gave a minimum failure stress prediction from the Design Curve in PD 6493, and these invariably lie outside the Failure Assessment Line. Those defects which gave a maximum failure stress prediction (from PD 6493) generally lie inside the Failure Assessment Line, in the safe region.

It should be noted, that in Figure 4.11 (b), the results of both UT inspection programmes are shown, and as noted in the preceding Section, the results of the second inspection programme gave more accurate predictions of defect criticality. Thus, for these more accurately predicted sizes, both the defect which gave the minimum PD 6493 failure stress, and that which gave the maximum PD 6493 failure stress defined (with only one exception) unsafe conditions in the Failure Assessment Diagram. Since the actual failure loads were used in the calculation of the S_r parameter in all cases, these assessment points should indeed all lie in the critical region; this serves once again to illustrate the improved accuracy of the second UT inspection.

4.4 Summary

This Chapter has reviewed some of the problems associated with welding, in particular the variability in microstructure and hence properties in a weldment, and the origin, nature and deleterious effects of welding residual stresses. Methods for artificially inducing a given defect type into a predetermined location in a weldment have also been described. The main emphasis of this Chapter, however, was the description of an experimental test programme, carried out with the aim of comparing fracture mechanics predictions of failure stress levels and defect criticalities, with actual observations.

The results obtained in the destructive testing of these defective weldments indicated, that for these particular specimens, the welding residual stresses did not affect the failure loads to any great extent. Consistent with previous published work in this field, in the four weld metals under consideration, (MMA and SA as-welded and stress-relieved) the factor of conservatism inherent in the Design Curve of the PD 6493 approach was calculated to be about 2 between recorded failure loads and those predicted from actual defect parameters.

The relative defect criticality of each of these weldments was also assessed using the Two-criteria, or R-6 Failure Assessment Diagram. These results indicated that the original R-6 Failure Assessment Line appears somewhat conservative with regard to failure conditions in both weld metals in both the as-welded and the stress-relieved condition. Accordingly, Failure Assessment Lines, based on these experimental results, have been postulated.

Two separate UT inspection programmes were performed on these test plates and the ultrasonic predictions of defect size and position were used as input data in each assessment method, and the results obtained were compared to those calculated for the actual defect in each testplate. It was shown that, for these weld metals, there appears to be some tolerance in both assessment procedures to significant variations in defect size predictions. However, the improved accuracy observed in the UT defect size predictions in the second inspection programme (which involved a specified sizing procedure, as opposed to the operators choosing their own preferred sizing procedure) resulted in more accurate fracture mechanics assessments of failure stress levels and defect criticalities.

Finally, it was shown that, within the limits of the analyses used, these two assessment procedures appear to give compatible results.

Table 4.1 : Measured failure loads and defect parameters

Plate Number	Condition	Failure Load (kN)	Defect Length (mm)	Defect Height (mm)	Critical Ligament (mm)	Effective Defect Parameter, $\bar{a}$ (mm)
1	As-welded	139,3	72	7	3,8	4,32
2	As-welded	135,2	71	9	4,5	5,45
3	Stress-relieved	132,2	63	10,4	4,2	17,09
4	As-welded	115,4	54	15	2,5	16,79
5	Stress-relieved	118,9	68	13,1	4,2	20,45
6	As-welded	137,5	63	7	6,0	3,79
7	As-welded	131,1	82	11	4,8	6,86
8	As-welded	125,8	73	12,3	5,2	21,69
9	Stress-relieved	120,3	65	15,5	5,4	21,25
10	As-welded	128,3	72	12,7	5,2	21,8
11	As-welded	126,8	79	7,2	4,9	4,21
12	As-welded	116,0	85	10,5	5,0	6,48
13	As-welded	115,3	85	11	4,0	21,34
14	Stress-relieved	106,3	75	15	4,6	23,93
15	Stress-relieved	123,3	68	15	4,2	21,54
16	As-welded	170,9	77	8,5	2,2	14,74
17	As-welded	140,5	82	12,5	1,5	19,7
18	As-welded	148,8	86	12,1	2,6	21,13
19	Stress-relieved	136,7	75	15,3	3,7	23,8
20	Stress-relieved	138,4	66	18,7	3,1	22,2
21	As-welded	167,5	81	11,6	2,9	20,34
22	As-welded	121,0	76	12,8	1,8	20,1
23	As-welded	119,3	78	14,3	2,5	22,63
24	As-welded	133,0	69	16,1	2,2	21,89
25	Stress-relieved	105,4	86	19	2,7	25,26
26	As-welded	146,6	73	9,6	2,2	16,28
27	Stress-relieved	114,4	78	12,3	3,1	20,8
28	As-welded	121,8	82	12,9	2,3	21,8
29	Stress-relieved	105,5	81	16	3,0	25,8
30	As-welded	107,0	77	19	2,5	28,65

Note: (1) Testplates 1 to 15 inclusive were MMA welded, testplates 16 to 30 inclusive were SA welded.

(2) Effective defect parameters in excess of 10 mm indicate that the embedded defect was recategorised to a surface defect.

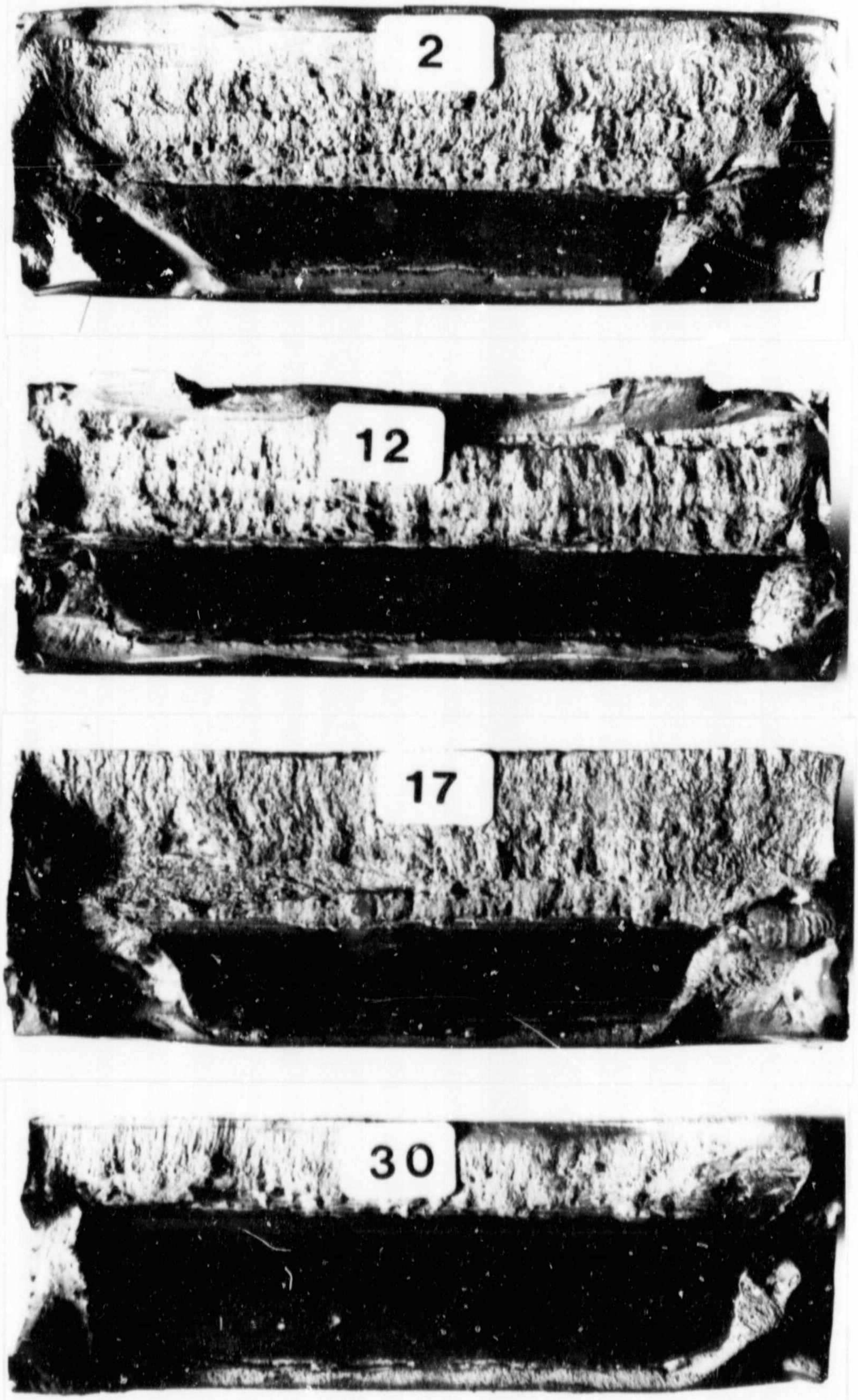

Figure 4.1 Typical fracture surfaces of the defective weldments fabricated for this study. Note the wide range in defect sizes that was achieved (magnification 1,5x).

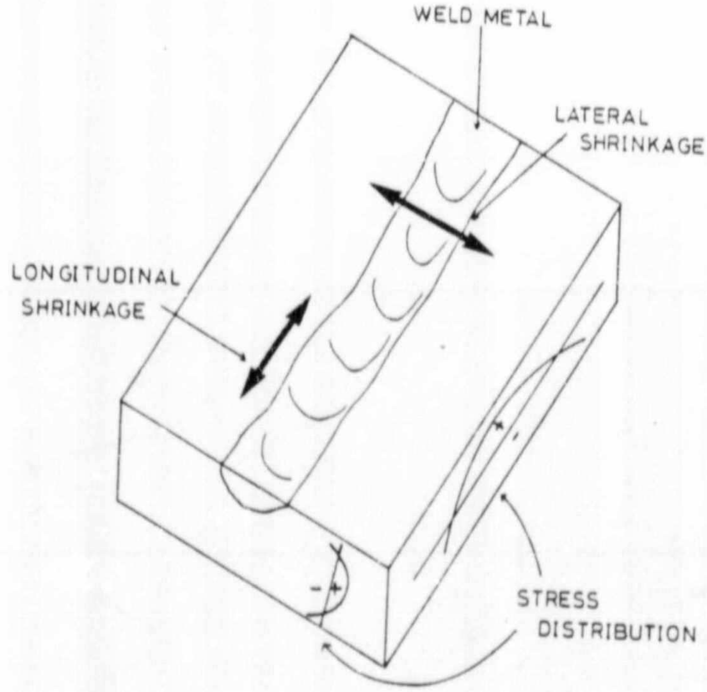

Figure 4.2 The through-thickness residual stress distribution due to the longitudinal and lateral contraction of a single weld run (from 84).

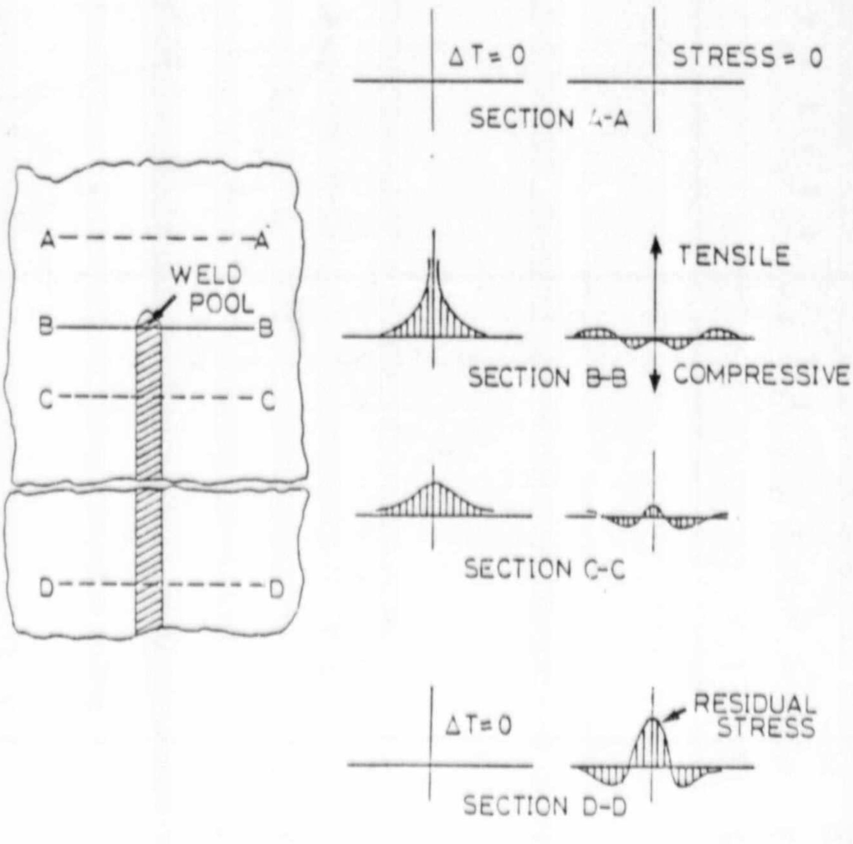

Figure 4.3 The temperature and stress gradients at different positions along a single weld pass (from 85).

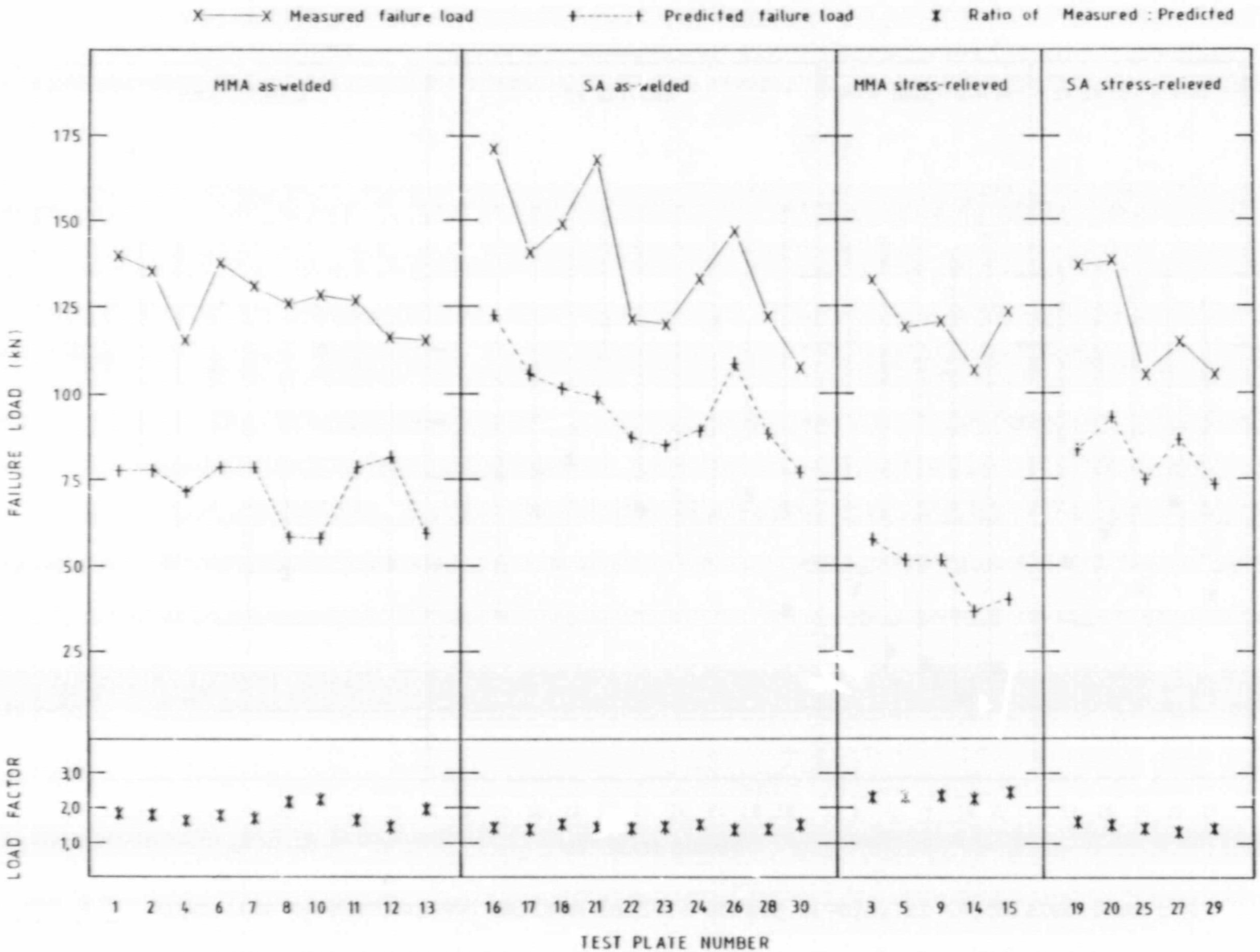

Figure 4.4 Comparison of measured failure loads and those calculated from the design curve, using the defect parameters measured from the fracture surfaces.

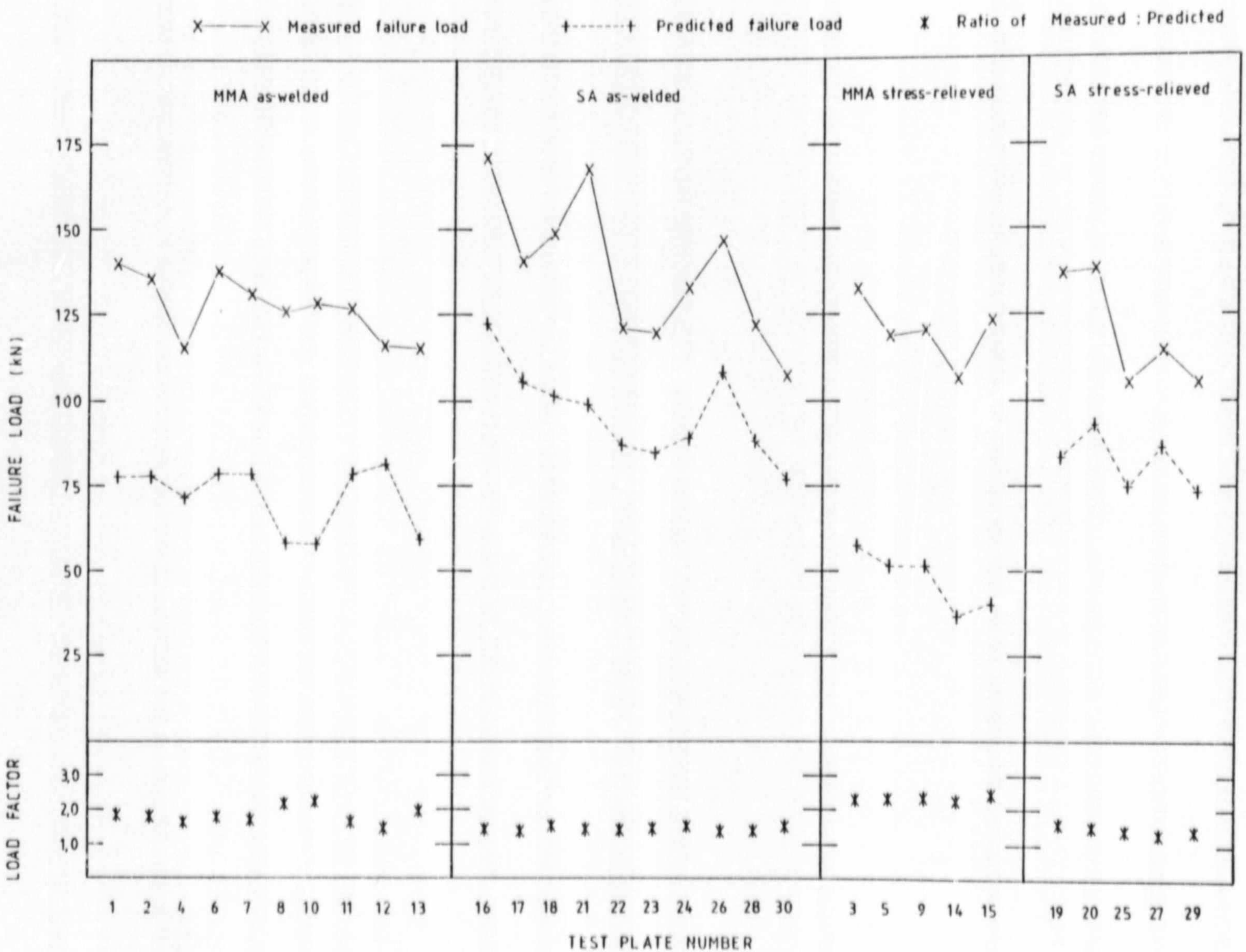

Figure 4.4 Comparison of measured failure loads and those calculated from the design curve, using the defect parameters measured from the fracture surfaces.

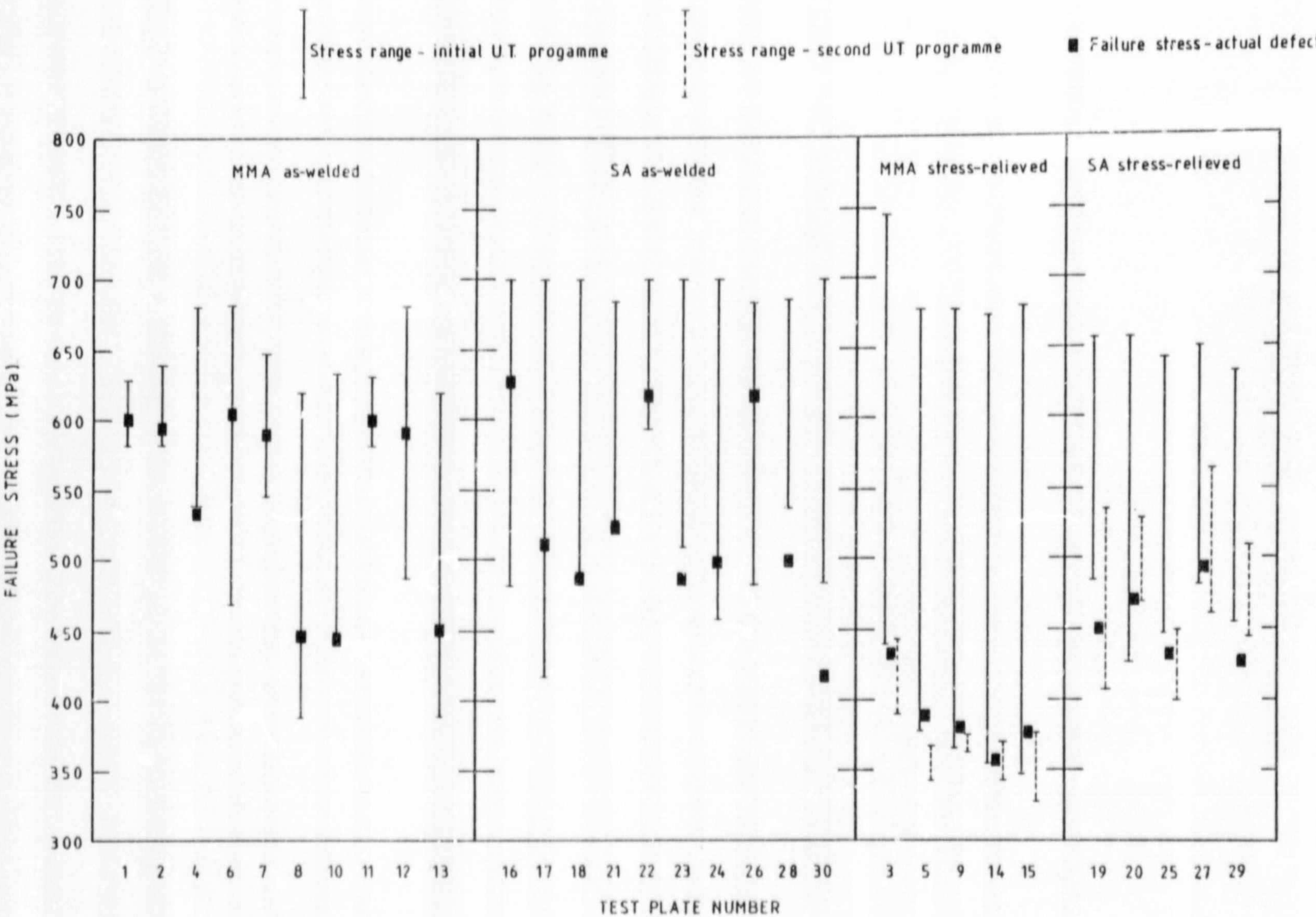

Figure 4.5 Comparison of minimum and maximum failure stress levels, as calculated from the UT defect size predictions, to the failure stresses calculated from the actual defect parameters. (The minimum and maximum failure stress levels were calculated from the maximum and minimum defect sizing estimates respectively).

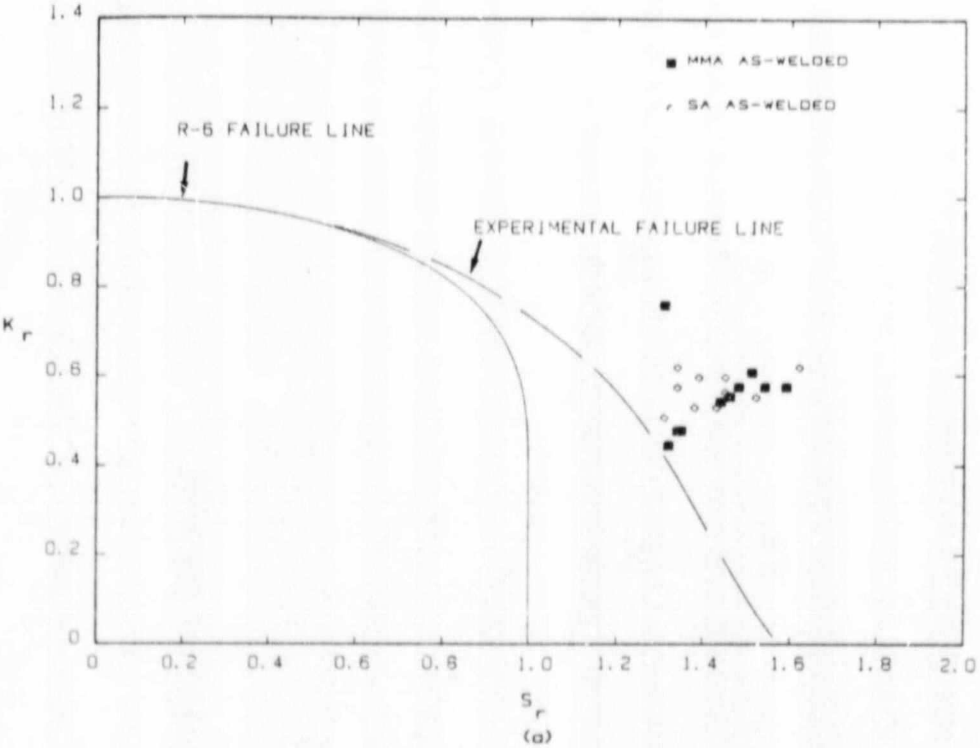

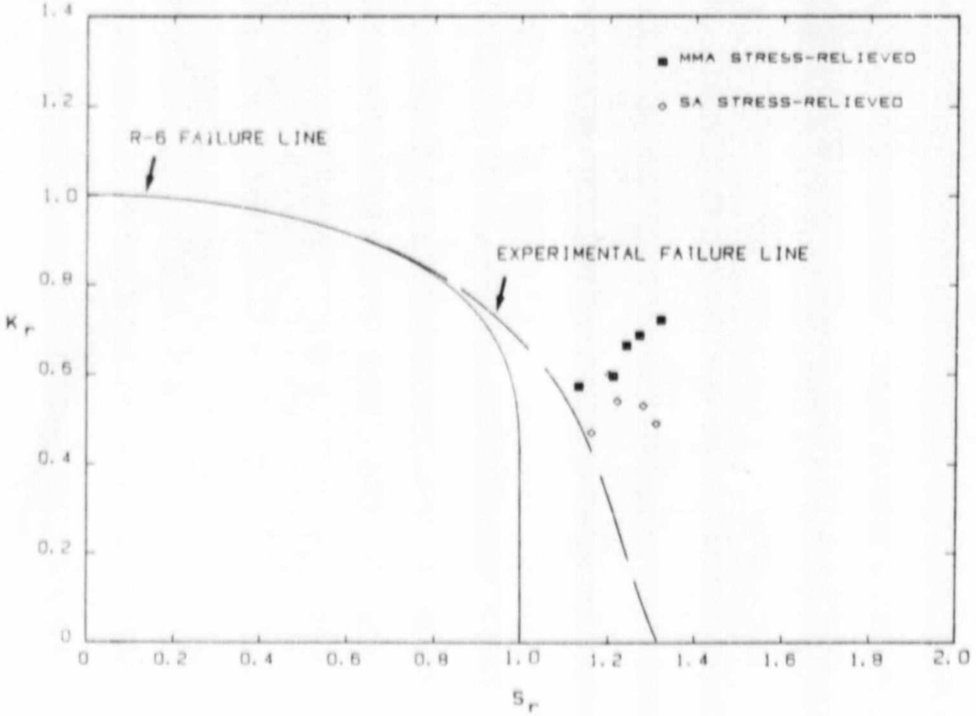

<u>Figure 4.6</u> The R-6 failure assessment diagram for the actual defect sizes in (a) the as-welded MMA and SA test plates and (b) the stress-relieved MMA and SA test plates.

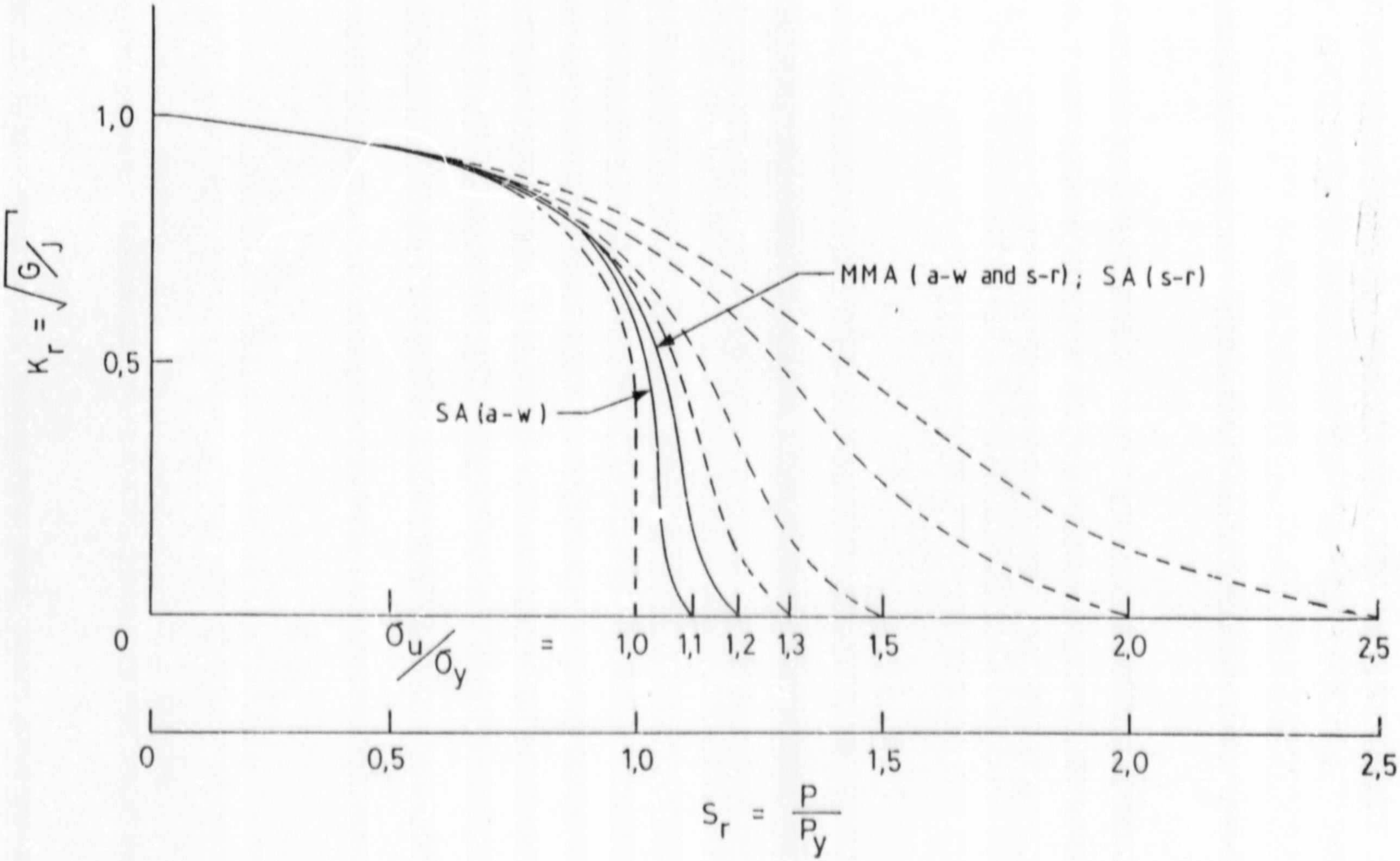

<u>Figure 4.7</u> The R-6 Failure Assessment Diagram, modified to take account of strain hardening properies (after Milne (61)). The solid Failure Assessment Lines correspond to those appropriate to the weld metals used in this study.

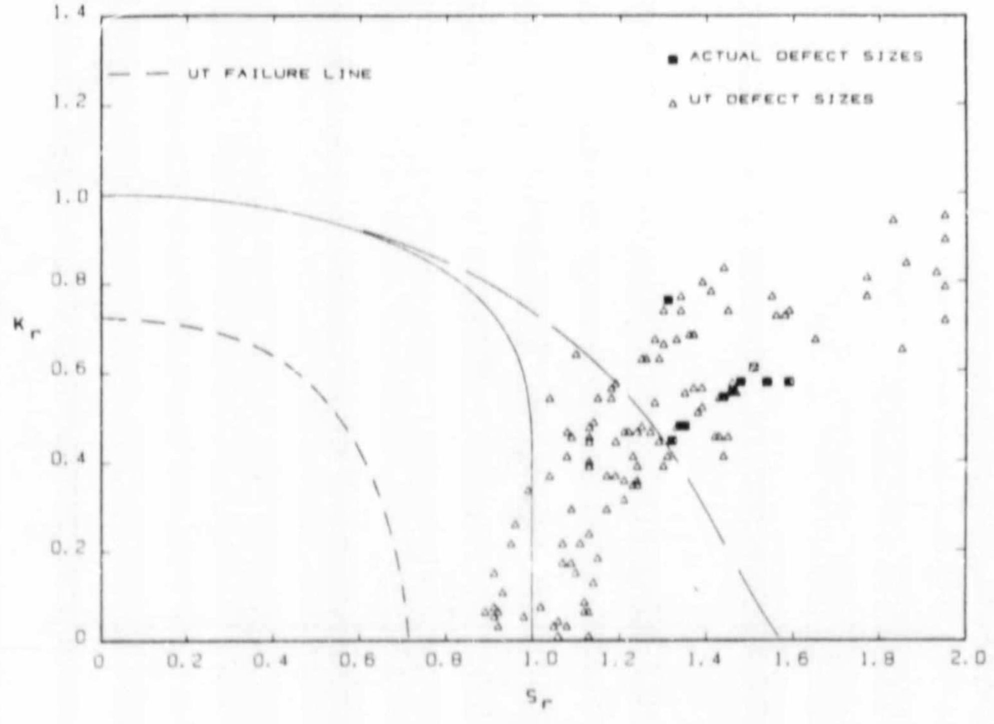

(a)

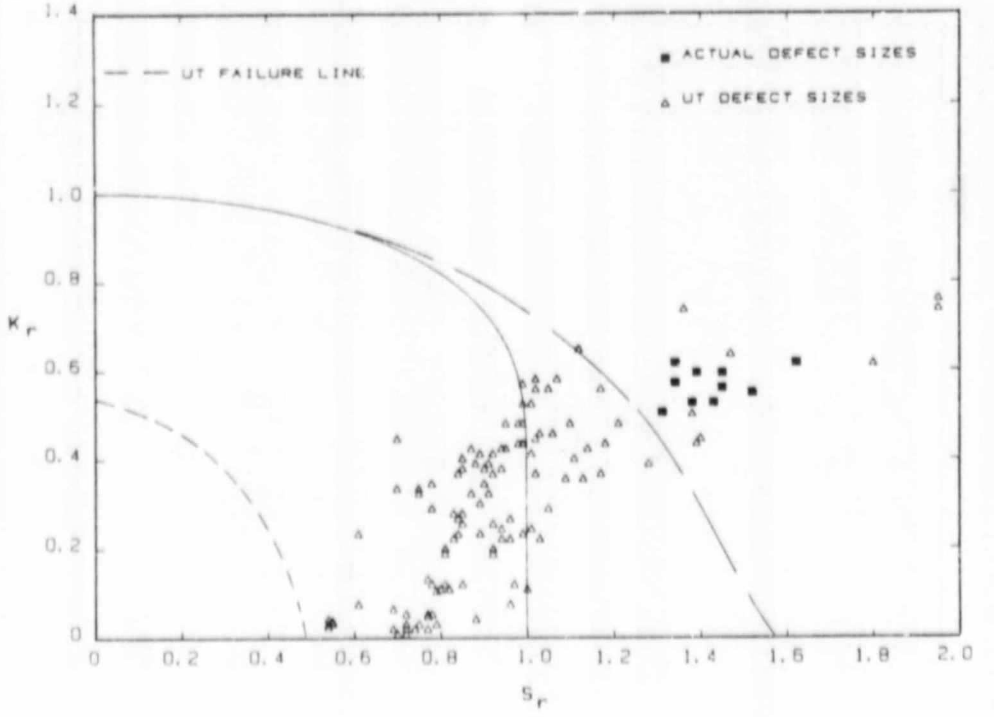

(b)

<u>Figure 4.8</u> The R-6 failure assessment diagram for the defect sizes predicted in the initial UT programme for (a) MMA as-welded series, and (b) SA as-welded series.

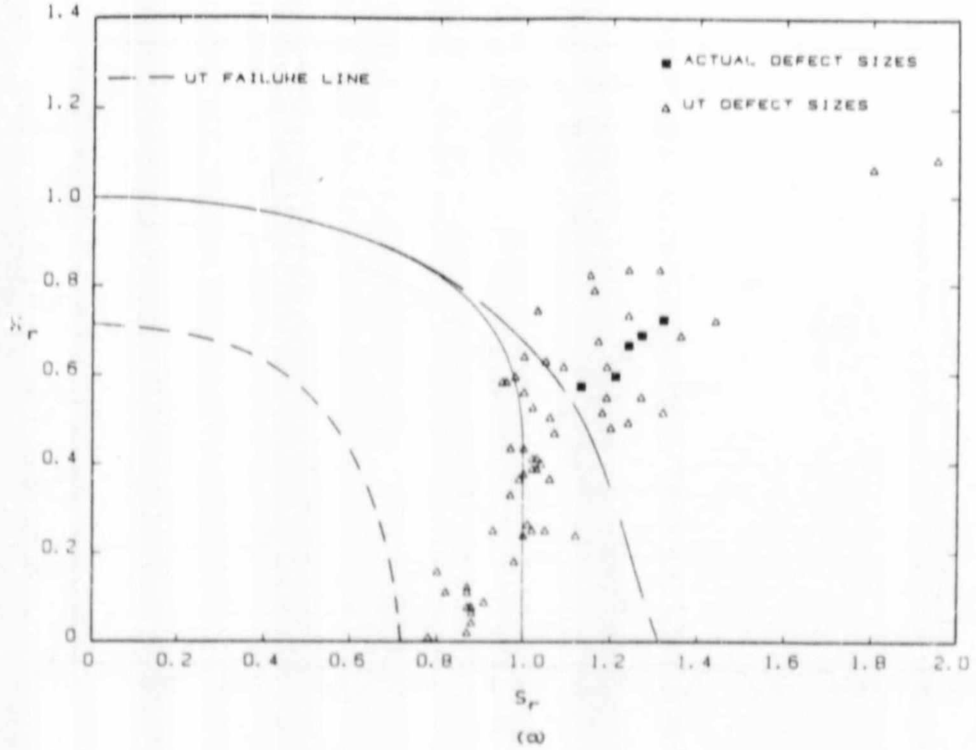

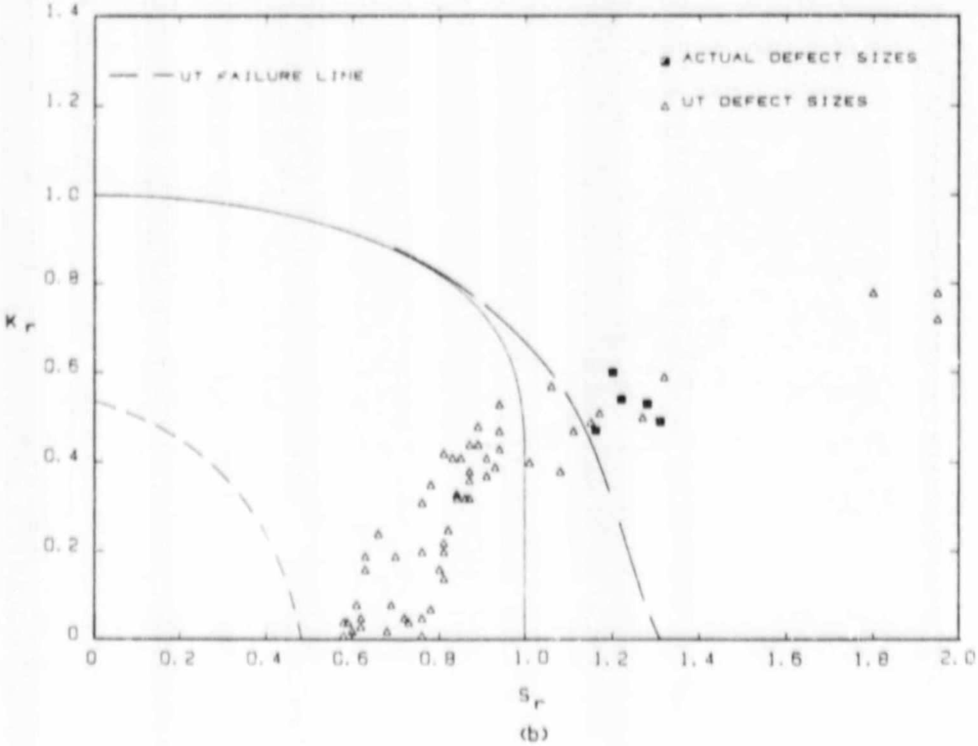

Figure 4.9 The R-6 Failure Assessment Diagram for the defect sizes predicted in the initial UT programme (a) MMA stress-relieved series and (b) SA stress-relieved series.

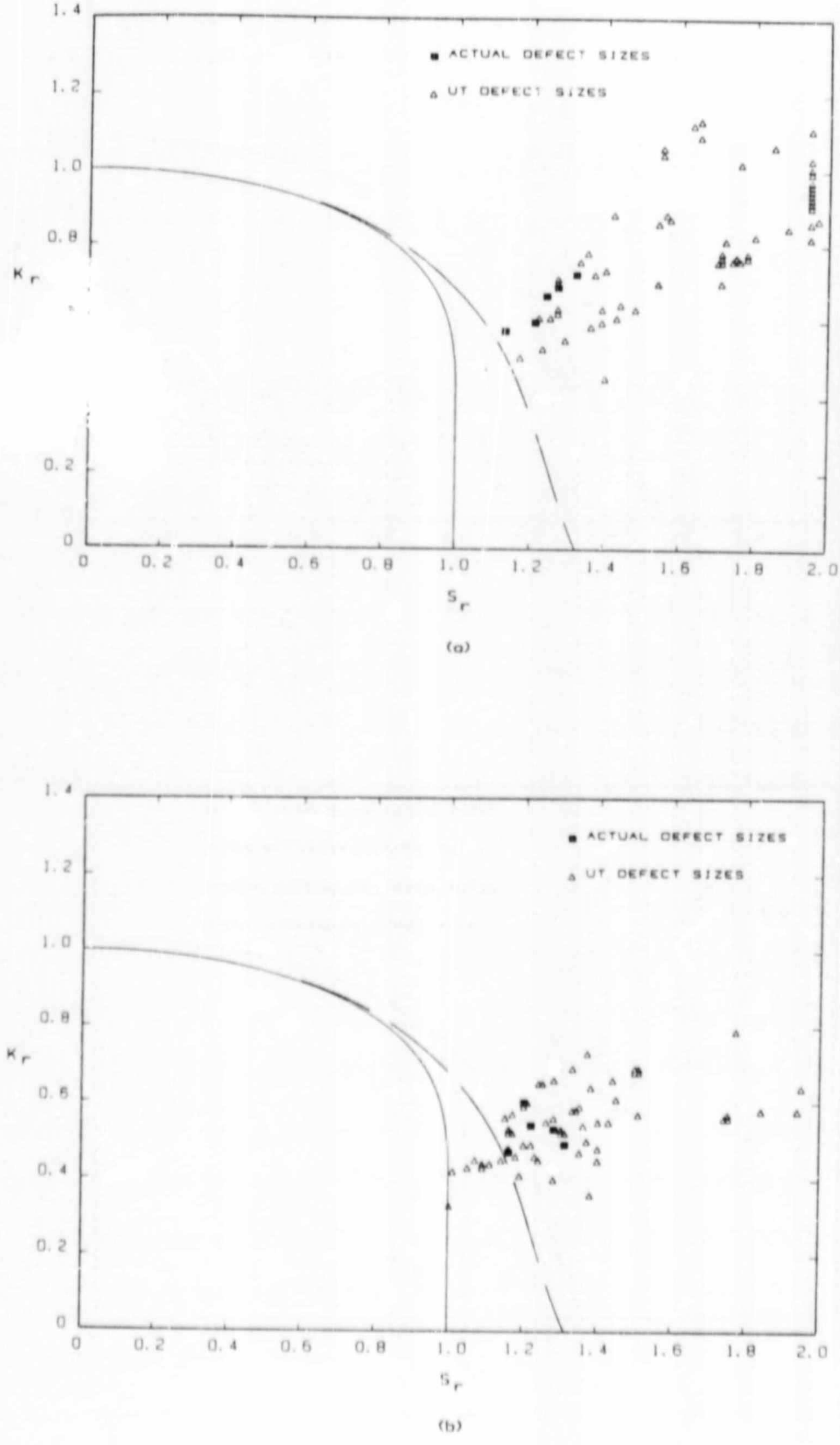

Figure 4.10 The R-6 failure assessment diagram for the defect sizes predicted in the second UT programme for the stress-relieved specimens (a) MMA series (b) SA series.

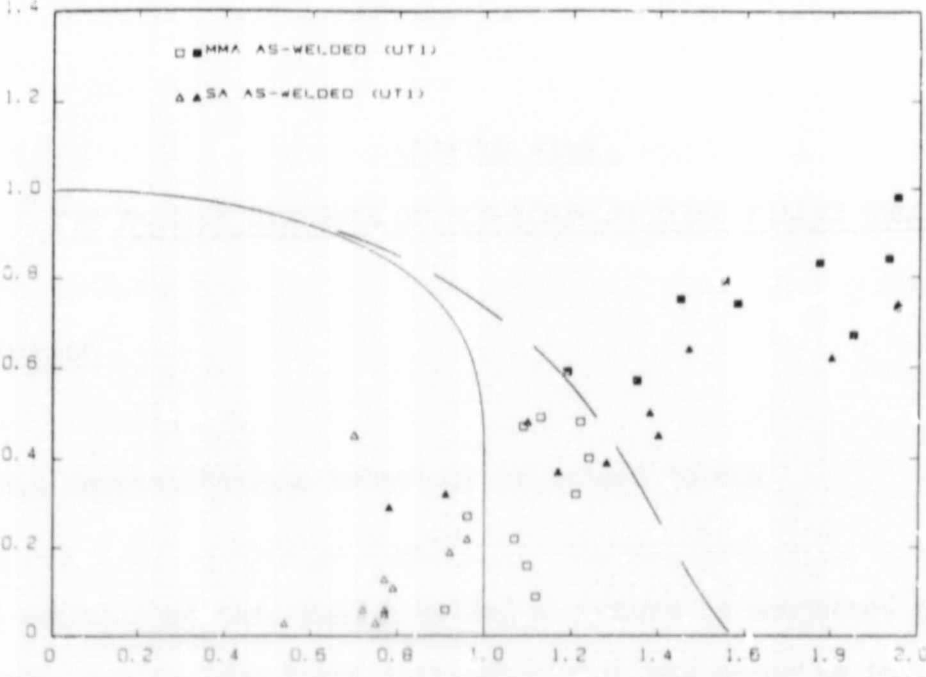

(a)

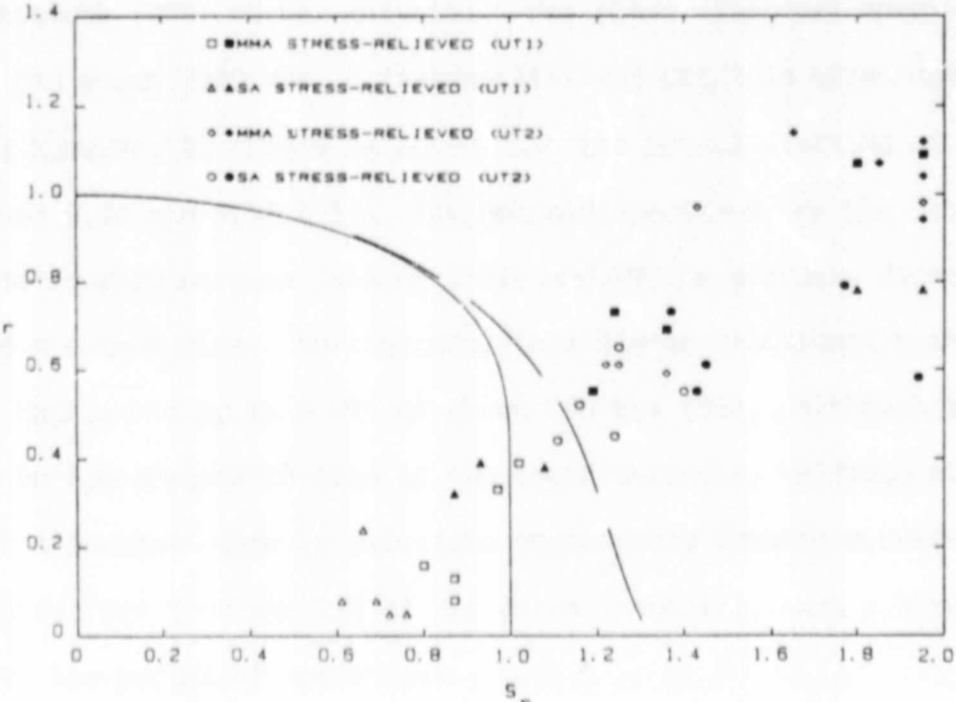

(b)

FIGURE 4.11 The R-6 failure assessment diagrams for the defects which gave predictions of minimum PD 6493 failure stress levels (solid symbols) and the defects which gave maximum PD 6493 failure stress predictions (open symbols). UT1 and UT2 denote results from the first and second UT inspections respectively.

CHAPTER FIVE

THE FATIGUE STRENGTH OF NON-LOAD-CARRYING FILLET WELDS

5.1 Introduction

5.1.1 General fatigue behaviour of welded joints

It is well established that when a welded structure is subjected to dynamic service loads, any fatigue crack initiation that may occur is invariably associated with the geometrical discontinuities or notches in, or near, welded joints. It is also well known that the fatigue limit of plain (i.e. unnotched) steel specimens can generally be related as some linear function to the Ultimate Tensile Strength (UTS) of the material. For plain (ferrous) specimens, with a UTS less than about 1500 MPa, a fatigue limit of UTS/2 is often used as a "rule of thumb"; however, it should be noted that the actual fraction of the UTS can vary between 0,23 and 0,65 (95). For notched specimens, on the other hand, the linear relationship between fatigue limit and UTS is strongly dependent on notch acuity and specimen size. Furthermore, this linear relationship is only generally applicable up to a UTS of about 540 MPa (95). Although this latter value may be appropriate to some of the lower strength, weldable structural steels, if a designer were to calculate permissible dynamic service stresses for a welded structure from the UTS of the parent material, such a structure would have a very low period of operation!

As early as 1960 it was shown that short, sharp defects at the weld toe have a very significant effect on the subsequent fatigue life of a welded joint (12). This effect was later examined in more detail, and in 1967 Signes et al. indicated that the presence of slag intrusions and undercut defects at the weld toe were responsible for the observed tendency of welded joints to exhibit a common fatigue strength, independent of base material yield strength (13). More recently, a stress concentration factor of 27 was calculated for undercut defects at the toe of a non-load carrying fillet weld (14). (It should be noted here that toe defects can occur in both fillet- and butt-welded details). It was also noted (13) that the fatigue crack initiation points were located in the region of weld metal that has been heated to a "pasty" condition during the welding process.

It is widely accepted that, due to the presence of such defects, there is no initiation stage in the fatigue cracking in welded joints, and that the cracks essentially propagate from the first loading cycle (see, for example, references 14,96-98). This then explains why welded joints in the higher strength steels do not show an improved fatigue life when compared to the lower strength steels, since resistance to fatigue crack propagation is relatively unaffected by tensile properties (99).

The general fatigue behaviour of welded joints has been examined extensively (see, for example, references 12-15, 18-23 and 95-102) and this has resulted in the Welding Institute (UK) publishing design rules for welded steel joints (18). This reference document provides a guide for the classification of all common weld details, and can be used to predict the fatigue life of a particular class of welded joint at various applied stress ranges. It is of interest here to note that the only stress parameter used in this reference document is the applied stress range, and no account is taken of the stress ratio, or the mean stress. The basis for this assumption is that, in the as-welded condition, high tensile residual stresses are liable to exist at the points of fatigue crack initiation. Thus, the real stress range will essentially pulsate downwards from the tensile yield stress. This point will be addressed further in section 5.1.2, to follow.

From the foregoing discussion, it is clear that in order to improve the fatigue strength of welded joints, it is necessary to remove the preferential crack initiation sites, and, if possible, introduce an initiation stage in the growth of the fatigue crack. Clearly, the area of interest will be the weld toe.

5.1.2 Welding residual stresses and fatigue strength

As mentioned above, the fatigue design rules for welded steel joints (18) do not account for the level of mean stress or the "R-ratio", which is defined as the ratio of the minimum stress divided by the maximum stress. This would seem to contradict the generally accepted view that high strength, low toughness microstructures (such as those found in the near heat affected zone in steel weldments) are strongly influenced by changes in R-ratio. Thus, for high strength, low toughness alloys, an increase in the R-ratio has been shown to increase the incidence of "static" modes of failure, thereby increasing the rate of fatigue crack propagation (54,103). Clearly, tensile residual welding stresses will increase the mean stress level, and as the mean stress is increased, the R-ratio increases.

It is therefore pertinent to consider the advantages and limitations of stress relief by heat treatment. Two cases of fatigue loading are considered, as shown schematically in Figure 5.1; fully reversed ($R = -1$), and fully tensile ($R = 0$). If the stress range is the same for the two different conditions, the fully reversed loading condition will be the least damaging, since the compressive portion of the applied loading cycle will not contribute to crack extension (Figure 5.1 (a)). However, it can be seen (Figure 5.1 (b)) that the effect of a tensile residual stress will be to increase the mean stress level, with the only limitation that the maximum stress in the fatigue cycle does not exceed the yield stress of the material. In this instance, the nominal fully reversed loading condition will be as damaging as the fully tensile condition.

It is estimated that, even after a heat-treatment stress relief, 10 to 25% of the welding residual stresses remain in a structure (87). Thus, as shown in Figure 5.1 (c), even after such a stress relief, the <u>nominally</u> fully reversed loading may still be as damaging as the fully tensile condition. It has been shown that only for fully reversed loading, where the stress ratio is -1, (i.e. applied loads always compressive) will stress-relieved joints generally have higher fatigue lives than as-welded joints (100). For positive applied stress ratios (i.e. fully tensile loading), on the other hand, a heat-treatment stress relief had little effect (100). This is the main reason why the Welding Institute (UK) favour mechanical dressing procedures such as grinding or peening rather than a heat treatment stress relief (which for a large structure may be prohibitively expensive). It must be emphasized that this argument is applicable specifically to increasing the fatigue strength of a welded structure; a heat treatment stress relief is often an effective procedure when potential problems of brittle fracture are under consideration. In such a situation the stress-relief will act to increase the level of static stresses required for fast fracture; however the influence of this tempering treatment on microstructure and therefore properties must also be carefully evaluated.

5.1.3 Techniques for improving weldment fatigue strength

Procedures which modify the weld toe profile, such as grinding, peening and TIG dressing, have been the subject of some considerable research and have been shown to significantly improve the fatigue life of fillet welded joints (see, for example, references 20-23). These methods may be implemented at relatively low cost, particularly in comparison to the heat-treatment stress-relief of full-scale structures, which may in any case be ineffective, as outlined above.

In general, these improvement techniques rely on one of two principles; the first obviously being the removal of defects at the weld toe by machining, as in the case of grinding, or by remelting the weld toe using TIG or plasma arcs. The second principle is to create compressive residual stresses at the weld toe, by cold-working, as in the case of peening. This can also be achieved by using a gas flame to heat a region some distance away from the weld, producing a tensile residual stress at that point, and therefore compressive residual stresses at the weld toe. Peening has the added advantage, however, that if the cold working operation treats the defect at the weld toe, the notch severity will also be reduced. The effectiveness of these post-welding procedures are well illustrated in Figure 5.2, from which it is evident that the peening operations provide a greater improvement in the subsequent fatigue performance than TIG remelting or grinding (22). Figure 5.3 compares the fatigue life of various ground and peened specimens, and again, it is evident that peening is the more effective of the two methods (20).

However, it is evident that procedures aimed at removing weld toe defects (such as grinding) are more widely in use than those which rely on the introduction of residual stresses, such as peening (2 One possible reason for this is that it is less certain that peening will in fact be effective. Peening can be carried out either by hammering the surface, or by directing a high velocity stream of particles at it, and in hammer peening there is a choice between using a solid tool, or a bundle of needles. The latter may be more effective in achieving access to the weld toe, while the former will achieve greater deformation, and therefore higher compressive residual stresses will result (23). As shown in Figure 5.2, the single point peening does seem to provide a greater improvement in fatigue strength (22). However, the degree of hammer peening is hard to standardise, since this is obviously affected by operating variables, such as hammer performance and operator technique, and the hardness of the material. It has therefore been suggested that the degree of peening be defined by the depth of deformation, and that the number of passes required to achieve 0,6 ± 0,1mm on a trial piece should be used on the actual weldments (20).

Clearly, the choice between grinding and peening will also be dependent on whether or not there is adequate access to the detail. The pneumatic hammer typically used for peening must be directed at the weld toe, and more than a single pass is necessary to achieve the required degree of weld profile modification. The peening tool is hard to control unless the operator can use his body weight to maintain the tool on the weld toe. A grinding operation, on the other hand, can be carried out in areas of restricted access, and the only limitation to this method is that the residual grinding marks must be parallel with and not perpendicular to the principal direction of the applied stresses. Finally, as evidenced in Figures 5.2 and 5.3, there is an increasing divergence from the as-welded S-N line with increasing life. Thus, the greatest improvement of fatigue performance is achieved in the low-stress, high-cycle range.

5.1.4 Fatigue cracking in large all-welded steel fans

As outlined i[illegible] One, fatigue cracking was shown to initiate from balance pad welds in large, all-welded steel fans during normal service. Initially, the balance pads were regularly stitch welded in position, as shown in Figure 5.4 (a), but these appeared to act as sites of stress concentration, since fatigue cracking which occurred in some of the fans were seen to be associated with these non-continuous welds (16). Accordingly, the fan manufacturers introduced a specification for the welding of balance pads, which includes rounding the corners of the attachment, applying a local pre-heat of 150^{o}C, and welding continuously around the attachment, as shown in Figure 5.4 (b).

However, when applying the Welding Institute's Design Rules (18) to these two details, it was apparent that both welds would be classified as "G" type joints and were thus expected to have similar fatigue strengths. For this joint classification, the reference document gives a 10 million cycle endurance limit of 38 MPa, and a 20 million cycle endurance limit of 30 MPa (18). Since in a year of continuous operation, these fans can experience in excess of 300 million cycles, and since the strain gauge work (17) indicated that the dynamic service stresses could approach 33 MPa, there was some considerable concern with regard to the origin of the service fatigue cracking, and the fatigue behaviour of the balance pad weldments. An experimental test programme was therefore initiated to investigate the fatigue behaviour of simulated balance pad specimens.

It would be virtually impossible to reproducibly fabricate balance pad welds on site (where there may be restricted access to the weld area) without any undercutting or other defects at the weld toes. Indeed, an 87 mm long fatigue crack that had almost propagated the full depth of the shroud plate was discovered during a routine inspection of an Induced Draft (ID) fan in a power station. An investigation showed that poor on-site welding had been the main cause of this cracking (104). However, by grinding or hammer peening the weld toes, the surface defects can be easily removed, and a smoother weld profile is obtained. In addition, as described above, peening introduces surface compressive stresses, which further improve the fatigue strength of the welded joint. Therefore specimens that had been dressed, either by grinding or peening after welding, as shown in Figures 5.5 (a) and (b) were also supplied for testing.

A further practical fabrication problem is that on-site facilities for baking electrodes may not always be adequate. Thus, hydrogen could be absorbed into the weldment during fabrication. The problem associated with hydrogen uptake is that atomic hydrogen is soluble in austenite at all temperatures, but practically insoluble in ferrite or martensite. When the austenite transforms to ferrite (or martensite), the excess hydrogen is rejected and tends to collect at inclusions, pores and defects to form molecular hydrogen which cannot diffuse away and therefore builds up a high-pressure, which will be additive to the residual welding stresses (82). Alternatively, the hydrogen may reduce the cohesive strength of the steel, such that brittle fracture may take place even under relatively small strains (82). This type of material degradation is obviously also aided by the presence of tensile residual stresses due to welding.

In an attempt to obviate any hydrogen cracking problems, the manufacturers have proposed that all such on-site welding should be performed using 309 L austenitic stainless steel electrodes. Any hydrogen present would thus remain in the austenitic weld metal, which could also act to soak up hydrogen from the base material, and the potential for hydrogen cracking would be reduced. (Indeed, the use of 18/8/3 Cr-Ni-Mo austenitic arc welding electrodes is recommended in cases where hydrogen may be absorbed into the weldment, so that the austenite acts as a reservoir for any small amounts of hydrogen present (82)). Therefore, specimens that had been welded using a 309 L stainless steel electrode, and subsequently ground or peened were supplied for testing, so that any deleterious effects could be investigated prior to changing the on-site weld procedure.

5.1.5 Summary

This section has reviewed some of the characteristics of the fatigue behaviour of welded joints, and outlined some of the causes for the generally poor performance, irrespective of the base material, that has been observed. Techniques for improving the fatigue strength of welded details have been described; these methods either rely on removing the preferential crack initiation sites at the weld toes, or create a residual compressive stress field at the probable initiation site, or both. In addition, it has been shown that a heat-treatment stress-relief will not be as effective as mechanical dressing techniques for pure tensile loading applications.

The problem of fatigue cracking in large, all-welded steel fans has been outlined, and the remaining sections in this Chapter detail the results obtained in the endurance limit testing of fillet welded specimens which were fabricated to closely simulate the various balance pad weld procedures, the details of which have been described above. It is relevant to point out that the results of this investigation will be pertinent to <u>any</u> welded structure that is subjected to cyclic stresses during service.

5.2 Experimental Procedure

Specimens were fabricated to simulate both the stitch and the continuous types of balance pad welds. The balance pad length was varied from 50mm to 90mm, since it has been shown (101) that the length of the welded attachment can affect the fatigue strength of the detail. The balance pad thickness and width were kept constant at 12 mm and 40 mm respectively, and the load carrying plates were 300 mm long, 100 mm wide and 16 mm thick. In all cases the welds in this initial set of specimens were made using the Manual Metal Arc procedure, and a high tensile E7018 electrode.

Originally, these fans had been fabricated from ROQ-tuf AD 690, a low alloyed quenched and tempered, weidable steel. The fans are now also being fabricated from BS 4360 Grade 55E steel, which has a considerably lower yield stress, and is thus more easily formed. However, in some cases, the steady state service stresses and temperatures are such that the higher strength material has to be used. The specified compositional ranges and mechanical properties are shown in Table 5.1 for both steel types (the ROQ-tuf AD 690 data was presented previously in Chapter Two, but is included here for easy reference). Accordingly, test samples were fabricated from both these steels, in order to perform a full evaluation of the fan problem, although it was not expected that the different steels would affect the results to any great extent. (It has previously been shown (100) that even considerable variations in material yield strength have little effect on the fatigue propeties of an as-welded joint).

It was thought that the service dynamic stresses were due to bending of the shroud plate about the blade welds; accordingly the specimens were tested under four point bending, with the balance pad weld on the tensile surface, as shown schematically in Figure 5.6. All specimens were tested in a 100 kN Amsler Vibrophore, fitted with a Howden load controller. The Amsler is an electromagnetic resonance machine, and test frequencies of between 50 and 300 Hertz may be achieved, depending on the compliance of the specimen and loading arrangement. This "natural" test frequency can be decreased by about 40 Hertz by adding standard weights to the machine. The Howden control module will automatically maintain the required static load, and can be set such that it will trip out either after a pre-determined number of cycles, or due to a change in the test frequency. This latter feature was particularly useful since, as the fatigue crack initiated and grew in the specimen, the compliance of the specimen would increase, and the test frequency would decrease. Thus the test could be automatically stopped a short time after the initiation of the fatigue crack.

The strain gauge work performed on a fan in operation (17) indicated that the mean service stress was of the order of 150 MPa, and each specimen was subjected to 50 000 "start-stop" cycles, with a stress range of 150 MPa, about a mean stress of approximately 75 MPa. These loading cycles are intended to simulate the start-stop cycling experienced by the fans during dynamic balancing, as well as the other start-stop cycles that may be imposed on the fan during operation. Although it has been pointed out by the manufacturers that this number of start-stop cycles is well in excess of that experienced by a fan in typical service, there were no instances of crack initiation in any of the specimens due to this initial loading sequence.

The mean stress was then increased to 150 MPa, and the stress range decreased to a predetermined value, and the Amsler Vibrophore was set to run for 10 million loading cycles (or approximately 22 hours of continuous testing). In the event of any fatigue crack initiation, the specimen compliance increases, thereby decreasing the test frequency and the machine is stopped automatically. If crack initiation did not occur within this first 10 million loading cycles the stress range was increased by 10 MPa; this incremental increase in stress range was repeated every 10 million cycles until crack initiation was observed. Thus, the endurance limit of each detail was defined in this work as the highest stress range at which crack initiation did not occur within 10 million cycles.

The first test specimen (a stitch weld) was started at a stress range of 20 MPa, and after 10 million cycles (representing approximately 22 hours of testing at 130 Hertz) the stress range was increased to 30 MPa; this incremental increase in stress range was repeated every 10 million cycles, and cracking eventually initiated at a stress range of 120 MPa!

Quite apart from the unproductive nature of this extended test, it is likely that the large number of cycles at low stress ranges elevated the actual fatigue limit by the phenomenon of "coaxing". Thus, appreciable increases in the fatigue limits of strain-aging materials have been observed by testing for long periods just below the fatigue limit (105). Accordingly, in subsequent tests on as-welded specimens, an initial stress range of between 40 and 60 MPa was chosen, and this stress range was increased by 10 MPa every 10 million cycles until fatigue crack initiation occurred.

5.3 Initial Results

5.3.1 The influence of weld procedure

Eight stitch welded specimens and ten continuously welded specimens were supplied for testing (106). In this initial phase of the work programme, two stitch welded and two continuously welded specimens were strain gauged; these specimens were used to confirm that the magnitude of the actual stresses in the specimens, due to the applied bending loads, were consistent with those stresses calculated using beam theory (106). The results of the fatigue tests performed on the remaining fourteen specimens are summarised in Tables 5.2 and 5.3.

It can be seen from Table 5.2 that the endurance limit of the stitch welded detail was 50 MPa for four of the six specimens tested. In the case of T1, the atypically high initiation stress range of 120 MPa is most likely as a result of coaxing, as described in the preceding Section. The slightly anomalous result for specimen T13, on the other hand, may be ascribed to the inherent scatter in fatigue testing. As will be detailed in the next Chapter (see also reference 107), the fatigue cracking in these six specimens occurred on both sides of the welded attachment, and initiation was typically subsurface, at the corner of the balance pad.

The results of the tests performed on the continuously welded samples (Table 5.3) indicates that there is some considerable scatter in the results, with four specimens (T2, T4, T10 and T12) having an endurance limit below 100 MPa, while the remaining four specimens (T3, T5, T9 and T11) showed an endurance limit in excess of 100 MPa. However, examination of the fracture surfaces indicated that the fatigue cracking in the four specimens with a low endurance limit had initiated from undercut defects at the weld toe. The fatigue cracking in the specimens which had a relatively high endurance limit, on the other hand, was seen to initiate at several points, as evidenced by the presence of ratchet markings, which are indicative of a relatively low stress concentration effect. Unlike the stitch welded samples, fatigue cracking only occurred on one side of the balance pad in the continuously welded samples. These macro-fractographic features will be described in more detail in Chapter Six, to follow.

It is also evident from Table 5.3 that, whereas three of the four specimens in which undercut defects were seen to be present were fabricated from ROQ-tuf AD 690 steel, the four specimens which had endurance limits in excess of 100 MPa were all fabricated from the lower strength BS 4360 grade 55E steel. This could indicate that the 55E material is more weldable than the AD 690, but could also be entirely fortuitous.

Thus, these results indicate that the revised, continuously welded detail does not exhibit any improvement in fatigue strength, compared to the old stitch-welded detail, due to the presence of short, sharp defects at the weld toe. It is of interest to note that this was first illustrated in 1960, in the testing of beams with web stiffeners that had been welded, either transversely or longitudinally to the tension flange, as shown schematically in Figure 5.7 (12). It was shown that the results of the tests performed on the longitudinally welded stiffeners fell on a common curve, whereas there were two sets of results for the transverse specimens. It was found that the transverse welds that failed at relatively low stress ranges were rougher than those on the transverse specimens that exhibited a higher fatigue strength. In addition, careful examination revealed the presence of undercut defects at the toes of the welds that had failed at low stress ranges (12). Comparing Figures 5.4 and 5.7, it is evident that the transverse welded stiffeners can be compared to the continuous balance pad welds, and the longitudinally welded stiffeners to the stitch weld type. Thus, the results obtained in this study can be directly compared with those obtained previously (12), and it is seen that there are indeed two sets of fatigue data for the continuously welded samples; those which failed at low stress ranges, due to undercut, and those which were defect free and showed a high fatigue strength.

5.3.2 Microstructural and mean stress effects

When this initial phase of the work was completed (106), a fatigue crack which had initiated from a balance pad weld was discovered during a routine inspection of an Induced Draft fan in a power station. It was apparent that, although the welding appeared to be continuous around the balance pad, it was not performed to the manufacturers specification. The cracked portion of the fan was therefore cut out of the fan, and submitted for investigation (104). A hardness traverse was performed across the weld, and it was seen that the peak hardness in the near heat affected zone was in excess of 400 Vickers microhardness. In addition, it was seen that the near-heat affected zone had a coarse martensitic microstructure, indicative of very high cooling rates. For comparative purposes, two of the continuously welded samples that had been tested as described in the preceding Section were sectioned, and a hardness traverse was performed across these welds. These results are shown in Figure 5.8, and it is clear that the peak hardness in the specimen weldments do not exceed 350 Vickers microhardness. Furthermore the near-heat affected zone micostuctures in these specimens were not fully martensitic, indicating a slower colling rate. Thus, the balance pad welding performed on the fan was not representative of the continuously welded specimens supplied for testing. Accordingly, test specimens were welded in such a way as to simulate the on-site welding, including the use of a high welding current to promote undercut, in addition to cooling the test plates prior to welding to simulate the rapid heat-transfer that would be achieved in a fan balance pad weld, if a local preheat had not been applied.

The results of the initial test-work of this phase of the programme are summarised in Table 5.4. Due to the urgency of the investigation, a slightly different fatigue testing programme was used. Firstly, as in the previous tests, 50 000 start-stop cycles at a stress range of 150 MPa were applied, and then the stress range was decreased to 20 MPa for 3 million cycles. Thereafter, the stress range was increased in increments of 10 MPa every 3 million cycles, until a stress range of 50 MPa was reached. The tests were terminated after 25 million cycles at this stress range, and the samples fractured by sharp impact after cooling in liquid nitrogen, and the fracture surfaces examined for evidence of fatigue cracking. As shown in Table 5.4, it is evident that there is a synergistic interaction between undercut defects and a hard heat affected zone, such that the 10 million cycle endurance limit of this detail could be decreased to 40 MPa (i.e. below that of the stitch welds). However, specimens welded so as to contain either undercut or a hard heat affected zone only, did not show any fatigue cracking after the 34 million cycle tests.

This phase of the test programme was later extended to include an investigation of the mean stress effect (108). It will be recalled from Section 5.1 that it is widely accepted that the dominant parameter in the fatigue behaviour of a welded detail is the stress range, and that the mean stress does not affect the fatigue strength (18). It is clear that the level of residual stresses in the fans is much greater than that in the small test specimens, since although these fans are given a stress-relief heat treatment after static balancing, the dynamic balance pads are as-welded, and there would be more restraint in the fans than in the flat sample plates. There was some concern about this aspect, especially with regard to the fact that high residual stresses would tend to elevate the nominal R-ratio; it will further be recalled from Section 5.1 that the high-strength, low-toughness microstructures (associated with the heat affected zone) are particularly susceptible to changes in this parameter.

Therefore, in order to assess the effect of tensile residual stresses on the fatigue performance of the balance pad welds, a series of tests were performed at elevated mean stress, such that the peak stress in the fatigue cycle was equivalent to the yield stress (440 Mpa) of the parent plate material. (i.e. for a stress range of 40 MPa, a mean stress of 420 MPa was applied). For this series of tests, after the initial 50 000 start-stop loading cycles, the stress range was decreased to 20 MPa, and this stress range was increased in increments of 10 MPa every 10 million cycles until crack initiation occurred.

As described earlier in this Section, these specimens had been welded without a preheat, such that a hard near-heat affected zone was formed, and at high welding currents to deliberately induce undercut defects. The results obtained in this phase of the test programme (108) are summarised in Table 5.5; they clearly indicate that, at high mean stress levels the endurance limit of the (badly fabricated) continuous welds could be as low as 40 MPa. These results therefore confirmed the findings of the initial phase of this work; in addition to demonstrating that the high mean stress level (or magnitude of residual stresses) did not affect this endurance limit.

It should further be pointed out that, when testing these welded samples at a mean stress of 150 MPa and a stress range of for example, 40 MPa, the R-ratio is 0,76. On the other hand, at a mean stress of 420 MPa, and the same stress range, the R-ratio is 0,91. This relatively small increase in R-ratio would not affect the fatigue strength of the detail to any great extent. This effect is probably also influenced by the fact that the high strength, low toughness microstructure is only a very small portion of the total extent of the weldment.